

DYNAMICS OF G-BAND BRIGHT POINTS DERIVED USING TWO FULLY AUTOMATED ALGORITHMS

M. BODNÁROVÁ¹, D. UTZ², J. RYBÁK¹ and A. HANSLMEIER²

¹*Astronomical Institute, Slovak Academy of Sciences,
SK-05960 Tatranská Lomnica, Slovakia*

²*IGAM/Institute of Physics, University of Graz,
Universitätsplatz 5, A-8010 Graz, Austria*

Abstract. Small-scale magnetic field concentrations (~ 1 kG) in the solar photosphere can be identified in the G-band of the solar spectrum as bright points. Study of the G-band bright points (GBPs) dynamics can help us in solving several questions related also to the coronal heating problem. Here a set of 142 G-band speckled images obtained using the Dutch Open Telescope (DOT) on October 19, 2005 are used to compare identification of the GBPs by two different fully automated identification algorithms: an algorithm developed by Utz *et al.* (2009a, 2009b) and an algorithm developed according to papers of Berger *et al.* (1995, 1998). Temporal and spatial tracking of the GBPs identified by both algorithms was performed resulting in distributions of lifetimes, sizes and velocities of the GBPs. The obtained results show that both algorithms give very similar values in the case of lifetime and velocity estimation of the GBPs, but they differ significantly in case of estimation of the GBPs sizes. This difference is caused by the fact that we have applied no additional exclusive criteria on the GBPs identified by the algorithm based on the work of Berger *et al.* (1995, 1998). Therefore we conclude that in a future study of the GBPs dynamics we will prefer to use the Utz's algorithm to perform identification and tracking of the GBPs in G-band images.

Key words: photosphere - magnetic fields - image processing techniques

1. Introduction

The G-band is a molecular band-head in the solar spectrum at around 430 ± 1 nm, consisting of electronic transitions between rotational and vibrational sub-levels of the molecule CH. Images of the photosphere taken with a broadband interference filter in the G-band show isolated brightenings located inside and near the intergranular lanes with high contrast to their surroundings. It was found that these brightenings are caused by the presence of strong magnetic field concentrations (Berger and Title, 2001). Therefore these brightenings can be used as indirect tracers of the magnetic

field, thus they are known as magnetic bright points, located in intergranular lanes. They are also called bright points, network bright points, GBPs, when observed with a G-band filter, or filigree in an active network region. Several of the GBPs properties are quantified in former works, notably Muller *et al.* (1994), Berger *et al.* (1998) and Nisenson *et al.* (2003). Hence the GBPs are small scale magnetic features in the solar photosphere, which are important to be studied in order to understand the solar magnetism. In addition the GBPs play a crucial role in solar physics, firstly because they can store magnetic energy, and secondly because their motions can generate MHD waves which could contribute to the coronal heating.

Here we present a study of two different fully automated algorithms to identify the GBPs in the G-band images. The selection of the more suitable algorithm will help us make a further study of their dynamics more reliable.

2. Data

We used two data sets of speckle reconstructed images (Sütterlin *et al.*, 2001) of the quiet solar photosphere in the G-band (430 nm) and blue continuum (432 nm) recorded simultaneously with the Dutch Open Telescope (DOT) (Rutten *et al.*, 2004). The time sequences were collected on 2005 October 19, at 09:55–11:05 UT under good seeing conditions from a network region close to the disc centre. Both data sets consist of 142 images with a cadence of 30 s, each 1112 pixel \times 818 pixel in size and the sampling was 0.071 arcsec/pixel.

3. Identification Algorithms

We used two different fully automated algorithms to identify the GBPs of the G-band images.

The first algorithm developed by Utz *et al.* (2009a, 2009b) consists of 3 steps and it identifies and tracks the GBPs. The segmentation step is based on the idea of following contours of the features from their brightest pixels down to their faintest ones in subsequent steps. In the identification step the bright features (the GBPs) are determined by a size criterion. In the time series generation step the identified GBPs are tracked in subsequent images and their properties are analysed. During the tracking process some of the

identified GBPs are excluded, especially from the beginning and the end of the data set because they were not observed for their whole existence.

The second algorithm is based on works of Berger *et al.* (1995, 1998) and it identifies the GBPs themselves. At first a binary image is produced from a thresholded version of the G-band image. For every pixel of the image the value

$$B(x, y) = \frac{1}{(2M + 1)^2} \sum_{u=x-M}^{u=x+M} \sum_{v=y-M}^{v=y+M} I(u, v) - \frac{1}{(2N + 1)^2} \sum_{u=x-N}^{u=x+N} \sum_{v=y-N}^{v=y+N} I(u, v)$$

is calculated, where M and N are integers, $M < N$ and $I(x, y)$ is the intensity of the image at the pixel location (x, y) . All pixels with B above a specific threshold are set to 1 and the rest is set to 0. This step allows us to eliminate most of the residual granulation noise. A second binary image is produced from the G-band/wide band difference image (G-band image – blue continuum image). Again all pixels above another specific threshold are set to 1 and the rest is set to 0. This step allows us to select only the GBPs pixels and the pixels exhibiting the "diffuse" G-band component.

The two binary images are combined in a boolean "and" operation to eliminate most granular peaks and produce a GBPs binary image. The identified GBPs are then tracked in GBPs binary images using the third step of Utz's algorithm.

4. Results

Identification of the GBPs in the G-band images using both algorithms seems to work as it was anticipated (Figure 1). The total number of identified GBPs in all 142 G-band images was 38140 for Utz's algorithm and 43639 for Berger's algorithm. After the identification process the obtained GBPs with both algorithms were traced in time using the "Time series generation step" of Utz's algorithm. In the case when the identification of the GBPs was performed, using Utz's algorithm, we have obtained 26238 identified GBPs, resulting in 4017 individual GBPs tracked in time on the subsequent G-band images. In the case when identification was performed

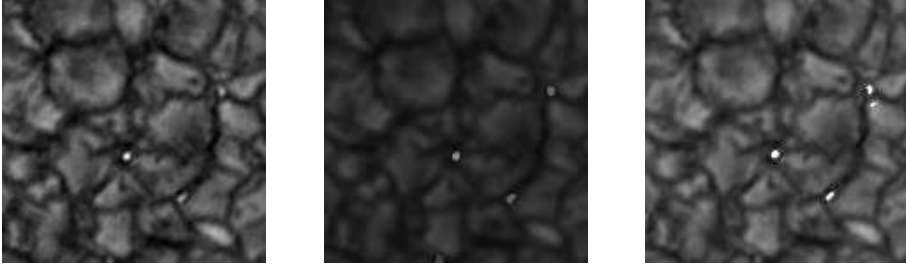


Figure 1: Example of identification of the GBPs: the G-band image (left), identification with Utz's algorithm (middle) and with Berger's algorithm (right). A typical example of misidentification of a part of a granule for a GBP is the bright smear under the uppermost GBP on the right image.

using Berger's algorithm 30234 identified GBPs were recorded leading to only 3900 individual GBPs tracked in time.

Both of the algorithms create different misidentifications when they identify parts of a granule as a GBP (for example see Figure 1).

We studied in detail some properties of the tracked GBPs identified with both algorithms focusing on their lifetimes, sizes and velocities.

We obtained quite similar lifetimes for both algorithms. The mean lifetimes were measured to be 3.00 ± 2.72 min for Utz's algorithm, and 3.52 ± 3.49 min for Berger's algorithm.

We compared the obtained size distributions of the tracked GBPs for both algorithms (Figure 2). The result showed that the size distribution of the GBPs in the case of GBPs identification using the Utz's algorithm is in good agreement with previous estimations obtained by other authors (Berger *et al.*, 1995; Utz *et al.*, 2009a). In the case of Berger's algorithm, the mean value of the size distribution is shifted towards smaller values and the whole distribution is broader. This is caused by the fact that in the case of Berger's algorithm we did not apply any size criteria on the identified GBPs and we have not excluded any of them (not even the ones consisting of only one pixel). Another possibility for this difference is the effect of speckling which can produce an additive noise in intensity pattern on small scales.

In the case of the velocities of the tracked GBPs obtained for both identification algorithms the obtained values are quite the same (Figure 3) and they correspond nicely with previous results of other authors (Muller *et al.*, 1994; Berger *et al.*, 1998; Nisenson *et al.*, 2005, Utz *et al.*, 2009b).

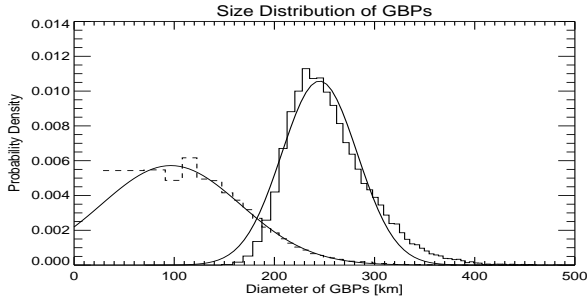


Figure 2: Size distributions of the tracked GBPs: identification with Utz’s algorithm (solid line) and with Berger’s algorithm (dashed line). The histograms are fitted by a solid line gaussian.

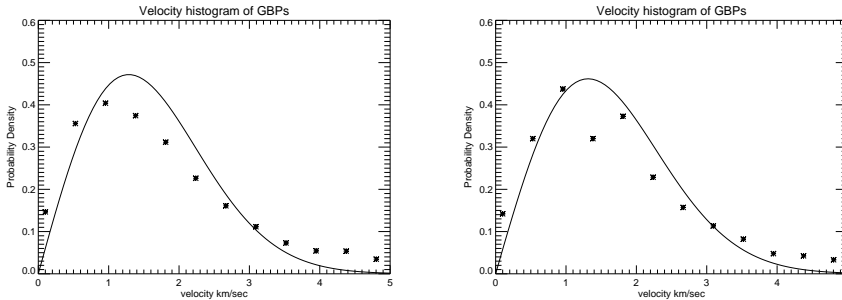


Figure 3: Distributions of the velocities of the tracked GBPs: identification with Utz’s algorithm (left) and with Berger’s algorithm (right).

5. Conclusions and Future Plans

We performed an analysis of two different fully automated algorithms for identification of the GBPs in the speckled G-band images in order to find out which of the two gives more reliable results according to present knowledge on the GBPs. Our analysis showed that both algorithms give comparable results (especially in case of velocity estimations we are most concerned) for the same data set of the G-band images. In the case of Berger’s algorithm the final number of the tracked GBPs is lower than in the case of Utz’s algorithm despite of the greater number of the identified GBPs. Additionally, the size distribution obtained by Utz’s algorithm is more reliable than the size distribution obtained by Berger’s algorithm. Therefore, we prefer to use

Utz's algorithm in our further study of connection of GBPs dynamics to the coronal heating.

Acknowledgements

The authors acknowledge the support of the Slovak grant agency SRDA through the projects 0066–06 and SK–AT–0004–08. D. U. and A. H. thank for the support of the Austrian FWF grant: P20762. Observations have been funded by the OPTICON Trans–national Access Programme and by the ESMN–European Solar Magnetic Network – both programs of the EU FP6. The DOT is owned by Utrecht University and located at the Observatorio del Roque de los Muchachos of the Instituto de Astrofísica de Canarias.

References

- Berger, T. E., Löfdahl, M. G., Shine, R. A., and Title, A. M.: 1998, *Astrophys. J.* **495**, 973.
- Berger, T. E., Shrijver, C. J., Shine, R. S., Tarbell, T. D., Title, A. M., and Scharmer, G.: 1995, *Astrophys. J.* **454**, 531.
- Berger, T. E. and Title, A. M.: 2001, *Astrophys. J.* **553**, 449.
- Muller, R., Roudier, Th., Vigneau, J., and Auffret, H.: 1994, *Astron. Astrophys.* **283**, 232.
- Nisenson, P., Ballegooijen, A. A., de Wijn, A. G., and Sütterlin, P.: 2003, *Astrophys. J.* **587**, 458.
- Rutten, R. J., Bettonvil, F. C. M., Hammerschlag, R. H., Jägers, A. P. L., Leenaarts, J., Snik, F., Sütterlin, P., Tziotziou, K., and de Wijn, A. G.: 2004, in A. V. Stepanov, E. E. Benevolenskaya, and A. G. Kosovichev (eds.), *Multi-Wavelength Investigations of Solar Activity, IAU Symposium 223*, 597.
- Sütterlin, P., Hammerschlag, R. H., Bettonvil, F. C. M., Rutten, R. J., Skomorovsky, V. I., and Domyshev, G. N.: 2001, in M. Sigwarth (ed.), *Advanced Solar Polarimetry: Theory, Observation, and Instrumentation, ASP Conf. Ser.* **236**, 431.
- Utz, D., Hanslmeier, A., Möstl, C., Muller, R., Veronig, A., and Muthsam, H.: 2009a, *Astron. Astrophys.* **498**, 289.
- Utz, D., Hanslmeier, A., Muller, R., Veronig, A., Rybák, J., and Muthsam, H.: 2009b, *Astron. Astrophys.*, submitted